QUANTIFICATION OF FLOW CURVE HYSTERESIS DATA – A NOVEL TOOL FOR CHARACTERISING MICROFIBRILLATED CELLULOSE (MFC) SUSPENSIONS

MICHEL SCHENKER^{1, 2, 3}, JOACHIM SCHOELKOPF³, PATRICK GANE^{3, 4} AND PATRICE MANGIN¹

¹University of Quebec in Three Rivers (UQTR), 3350 Boulevard des Forges,
G9H 5H7 Trois-Rivières (Québec), Canada

²FiberLean Technologies Ltd., Par Moor Road, PL24 2SQ Par, Cornwall, England

³Omya International AG, Baslerstrasse 42, 4665 Oftringen, Switzerland

⁴Aalto University, School of Chemical Engineering, Department of Bioproducts and Biosystems,
Vuorimiehentie 1, 00076 Aalto, Helsinki, Finland

*Corresponding author: michel.schenker@fiberlean.com

Received: 4.1.2018, Final version: 13.3.2018

ABSTRACT:

A novel method is introduced to describe quantitatively hysteres is seen in flow curves of microfibrillated cellulose suspensions.Also, a data normalisation procedure is presented that allows a direct comparison of data from suspensions of different solids contents. The discussion of the flow curve hysteresis of an MFC suspension is proposed to provide a lot of information on the suspension morphology under flow. Such information is not only useful for process design, but also may serve as a quality control tool. Hysteresis data as a function of the suspension solids content are provided, and considered with reference to an overview made of peer work in the field. Two discrete hysteresis loop areas were found in the flow curves presented in this work, each associated with a distinct shear rate region, one where the viscosity of the flow curve during shear rate increase is higher than that of the shear rate flow curve at decreasing shear rate (named positive hysteresis) and another where it is the $opposite (named \ negative \ hysteres is). This \ behavior seems \ to \ have \ been \ rarely \ reported, and \ where \ reported \ we \ offer \ an \ explanation \ and \ where \ reported \ we \ offer \ an \ explanation \ and \ where \ reported \ we \ offer \ an \ explanation \ and \ where \ reported \ we \ offer \ an \ explanation \ and \ where \ reported \ we \ offer \ an \ explanation \ and \ where \ reported \ we \ offer \ an \ explanation \ and \ where \ reported \ we \ offer \ an \ explanation \ and \ where \ reported \ we \ offer \ an \ explanation \ and \ where \ reported \ we \ offer \ an \ explanation \ and \ an \ explanation \ explanation \ an \ explanation \ e$ nation, based on morphological models and rheometer measurement set up, as to why other researchers may find a variety of hysteresis forms. It is hypothesised that the negative normalised hysteresis is mainly depending on the excessive floccula $tion/s tructuration\ induced\ at\ intermediate\ shear\ rates\ during\ the\ shear\ rate\ increase,\ and\ that\ it\ is\ necessarily\ less\ with\ increased$ ing solids content because of the reduced availability of free water. The positive normalised hysteresis, however, is considered to originate from the different morphologies at lower shear rates, i.e. the initial, homogeneous structure vs. the structure that was previously induced by the intermediate shear during shear rate decrease. The positive normalised hysteresis appears not to depend on the solids content, indicating a self-similarity or scaling behavior of the structuring with respect to the underlying network structure.

KEY WORDS:

Microfibrillated cellulose, suspension, flow curve, hysteresis, morphology, quantification

1 INTRODUCTION

In recent years and currently, the potential for microand nanofibrillated cellulose materials (MFC, NFC) in various applications continues to be exploited intensively, not only by academia, but also by the industry [1–3]. The reason for this is the material's versatility, its interesting mechanical properties and of course the abundancy and sustainability of its raw feed source [4]. The coarser MFC grades (referring to the nomenclature proposal by Kangas et al. [5], whereby the term NFC should be used for materials containing only fibrils with width on the nanometre scale), are especially interest-

ing for high volume applications due to the lower production energy requirements that enable lower costs [6] and higher volume productions [7]. Whilst abiding by the definition of Kangas et al. [5], it is important to recognise that MFC itself will inevitably display nanofibrillation on the microfibre surface, leading on occasions to the term micro nanofibrillated cellulose (MNFC). As these grades naturally have a broad fibril size (widths) distribution, and may have different fibril morphologies depending on the fibrillation processes, individual products may exhibit differing sets of properties and each may be more, or less, suitable for a specific application.

To be able to select an adequate MFC product, a meaningful characterisation is necessary, and so lately also some effort is being put into developing procedures to classify the various MFC grades [5, 8]. The common findings are typically that a single characterisation method is not sufficient and that even a set of properties provides limited comparability for MFC grades of different origin, e.g. from different raw materials and/or derived via different pre- and post-fibrillation treatments. By getting a better understanding of the MFC (suspension) morphology, data obtained from different characterisation techniques may be understood better and more detailed interpretation may be possible. Even though rather indirect, rheological investigations can, if applied judiciously, provide essential insights into the suspension morphology. Therefore, the combination of direct and/or indirect imaging techniques with rheology measurement techniques are very strong tools to test hypothesised mechanistic models [9-12]. Yet, to be able to compare data of different studies, it is necessary to quantify the observed data and describe the used measurement parameters with an adequate level of detail. The latter is of special importance for MFC suspensions as they exhibit a complex rheology, including shear rate- as well as time-dependencies. These inherent properties in connection to the fact that they are at least two-phase (heterogeneous) hydrocolloids can lead to many measurementinduced artefacts, that also can depend strongly on the measurement parameters [13-15].

Whereas it is very common to report different viscosity numbers and storage and loss moduli, it is rare that further rheological properties are reported for MFC suspensions. Flow curves (viscosity as a function of shear rate) as well as amplitude and frequency sweep graphs are also provided sometimes [16, 17]. Several articles specifically investigate the rheology of MFC suspensions, commonly using shear rheometers [14, 18 - 22], but also pipe rheometers are used [23, 24], sometimes even coupled with additional techniques to get more direct information on the suspension morphology [10, 11, 22, 25]. A comprehensive and extensive review on recent developments in measuring the rheology of micro- and nanofibrillated cellulose suspensions is provided by Nechyporchuk et al. [26]. Yet, especially the information within flow curve graphs is typically not quantified. This is unfortunate, especially for a material like an MFC suspension that exhibits a very distinct flow behaviour, e.g. a discontinuous power law shear thinning flow curve, composed of different regions [17, 19, 27, 28]. A recent study by Schenker et al. [13] proposed several descriptors to describe quantitatively amplitude sweep measurements and flow curves, yet, only the shear rate increasing ramp of the flow curve is evaluated. This is especially highlighted because it was shown before, that MFC suspensions have different flow curves, depending on the direction of the shear rate profile, i.e. from low to high and vice versa. This behavior is expressed as the hysteresis areas between the two flow curves when they are overlaid [9, 19, 29]. As described by Martoïa et al. [9] and lotti et al. [19], this phenomenon can be attributed to different suspension morphologies, that originate from the different shear histories of the two flow curves. So, the hysteresis itself contains some information on the different morphologies at different shear rates, and therefore is a very promising property for deriving morphological models of MFC suspensions under flow.

The content of this work aims at comparing different approaches on how to describe the hysteresis in a useful way, and then to investigate those hysteresis derived properties in dependence of solids contents of the MFC suspension. The obtained data are tested statistically to identify whether potential trends are significant or not. Finally, the data are discussed with a view on existing morphological models of sheared MFC suspensions and a direct comparison made with hysteresis data seen from previous researchers' work. This work appears to be the first to propose the use of quantitative flow curve hysteresis data of MFC suspensions to derive mechanistic models. Further work is then carried out, to be reported in an upcoming study, to test the applicability of this promising characterisation method on different grades of MFC.

2 EXPERIMENTAL

2.1 MATERIALS

The materials used in this work are the same as those studied previously by Schenker et al. [13, 29]. As described previously, the MFC was manufactured by a purely mechanical process [29]. Briefly, bleached eucalyptus pulp was mechanically disintegrated as 3 wt% aqueous (tap water) suspension by means of an ultrafine friction grinder (Supermasscolloider MKCA 6-2, Masuko Sangyo Co., Japan). The method employs single passes at different grinder rotational speeds. The total electrical energy consumption normalised by the amount of dry cellulose matter, defined as the specific grinding energy, was 7.2 kWhkg-1. This process of mechanical fibrillation leads typically to a broad size distribution [10], i.e. containing both coarse fibres as well as individual fibrils (Figure 1). Thus, is it classified as MFC rather than NFC. In addition, since the MFC was not further modified, it forms a flocculated structure according to the description of Nechyporchuk et al. [26]. The starting suspension was diluted to 1, 1.5, and 2 wt% for

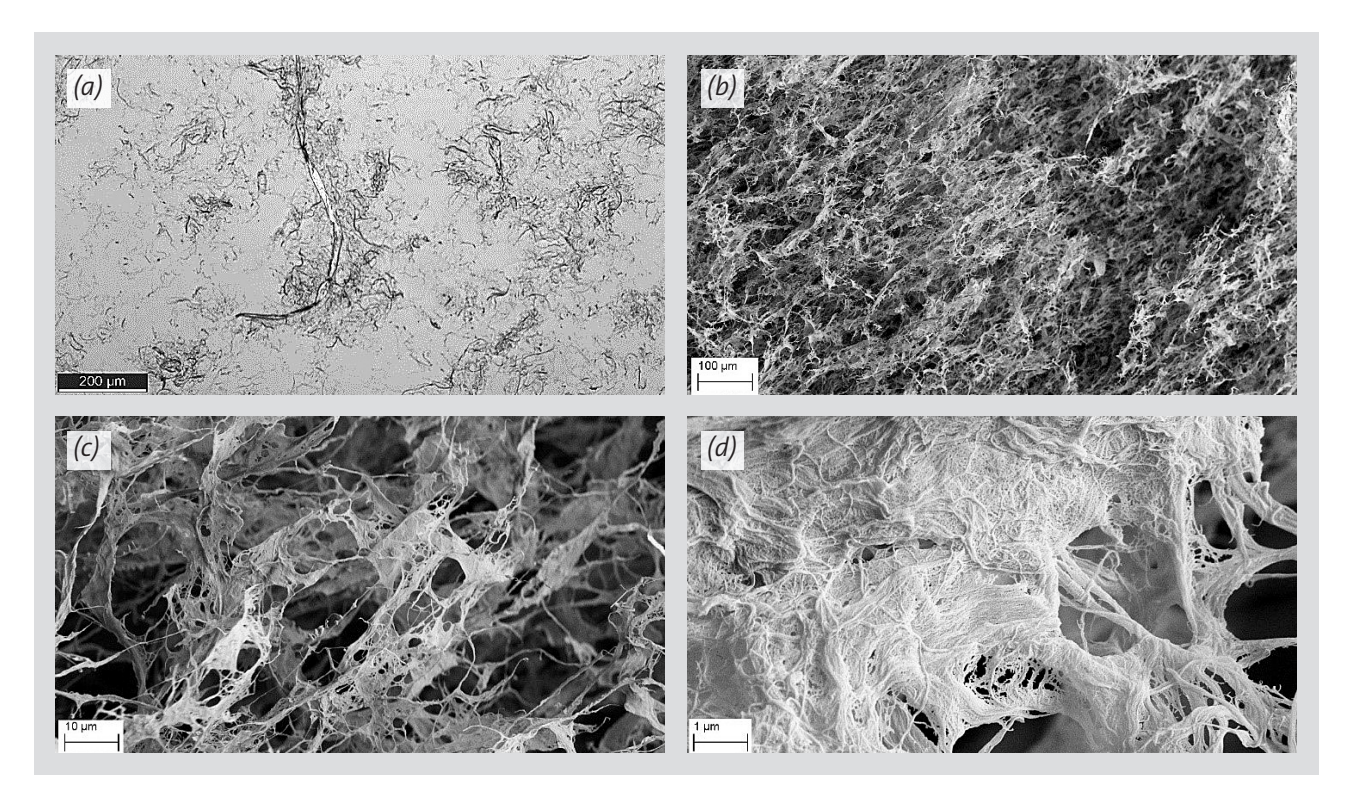


Figure 1: Optical microscopy image of MFC suspension at 0.5 wt% (a), and SEM images of freeze-dried aerogels from 0.5 wt% suspensions at increasing magnifications (b-d). Some left over coarse fibres are apparent, as well as some individual and isolated fibrils (Taken from Schenker et al. [13]).

use by further addition of tap water, followed by 2 min mixing at 12000 min⁻¹ (rpm) in a rotor stator mixer (Polytron PT 3000, Kinematica, Switzerland) followed by 5 min exposure in an ultrasonic bath. Prior to performing measurements, the diluted samples were left to stand for at least one hour.

2.2. IMAGING

Optical microscopy was the prime method of imaging (Axio Imager.M2m, Zeiss, Switzerland). Sample preparation consisted of diluting the MFC suspension to 0.5 wt% and then adding carboxymethyl cellulose (Finnfix10, CP Kelco, Finland), made down to 1 wt% solution as a dispersing agent, at an amount equivalent to 5 wt%, based on dry weight of MFC prior to mixing and ultrasonication. One drop of the prepared MFC suspension was placed between two glass slides for examination in the optical microscope. A second portion of the sample suspension was frozen in liquid nitrogen and freeze dried (Apha 1-2 LD Freeze Dryer, Martin Christ Gefriertrocknungsanlagen GmbH, Germany). A piece of the resulting aerogel was broken away from the sample and mounted on a support and sputtered with gold (8 nm) to enable imaging of the internal MFC aerogel structure by scanning electron microscopy (SEM) (Sigma VP, Zeiss, Switzerland).

2.3. RHEOLOGICAL MEASUREMENTS

All the measurements were performed on an MCR 300 rheometer (Anton Paar, Austria) at 20 °C, equipped with

a vane (six blades) in serrated (length profiled) cup system (vane: ST22-6V-16, diameter d_{vane} = 22 mm, cup: CC27-SS-P, diameter d_{cup} = 28.88 mm, profile depth = 0.5 mm, profile width = 1.65 mm), also supplied by Anton Paar (VS). This measurement system was selected because it appears to be less prone to produce measurement system-related artefacts, like shear banding or water depletion and connected apparent wall slip. In recent work, Schenker et al. [13] came to this conclusion by comparing different commonly used measurement systems and their influence on flow curve properties.

Flow curves (viscosity η in dependence of the shear rate $\dot{\gamma}$) were recorded by performing an automated shear rate increase ramp from 0.01 to 1 000 s⁻¹ directly followed by a shear rate decrease ramp from 1000 to 0.01 s⁻¹. 30 log- equidistant distributed point measurements were performed for each ramp, all with automated acquisition time mode and shear rate control. Further information on the automated acquisition time setting can be found in [30]. The tested shear rate points $\dot{\gamma}_i$ can be calculated according to

$$\dot{\gamma}_i = 0.01 \cdot 10^{\left(\frac{5}{29}\right)^{1-1}} s^{-1}$$
 (1)

Minimal and maximal acquisition times are 15.2 and 500 s respectively, however, typically only the first measurement point (shear rate of 0.01 s⁻¹) shows acquisition times around and longer than 300 s. The automated acquisition time setting is chosen, in order to let the suspension equilibrate at a given shear rate before deter-

mining the viscosity. This is of special importance in the transition region (non-power law region of the shear rate increasing curve "1" in Figure 2), where it is hypothesised that a dynamic aggregation process is taking place. A respective, detailed discussion was provided recently by Schenker et al. [13, 30]. For each of the 3 MFC suspension dilutions, 3 individual makedowns were produced, where each makedown was characterised from its own individual measurements which were repeated 3 times, creating 9 separate rheometer measurements per dilution.

Figure 2 shows a typical flow curve obtained in this work. The typical three region behavior can be seen for the flow curve of the increasing shear rate (curve 1) ramp-up [9, 13, 31], as well as the measurement set-up induced artefact at the very highest shear rates [13]. The flow curve of the decreasing shear rate (curve 2) rampdown does not exhibit such clearly defined regions, yet there are indications that also two different regions with different power law parameters can be found [19]. Very apparently, the two flow curves are not identical over the whole shear rate range, creating two separate hysteresis areas. At low shear rates, the viscosity of the increasing shear rate ramp-up is higher compared to the decreasing shear rate ramp-down at a given shear rate (+). The end of the positive hysteresis $\dot{\gamma}_a$ is defined as the last shear rate where the viscosity of the increasing shear rate ramp η_1 is larger than the viscosity of the decreasing shear rate ramp η_2 . At intermediate shear rates, the opposite can be observed (-), and, at even higher shear rates, there is no or only an insignificant difference between the two flow curves. The end of the negative hysteresis $\dot{\gamma}_h$ is defined as the first shear rate where the viscosities of both flow curves are again about the same. To characterise the hysteresis, the following approaches are introduced.

The first method aims to describe the actual hysteresis area, i.e. the actual area between the two flow curves. For the sake of simplicity, the area is not analytically integrated, but the trapezium rule approximation is employed, where the individual trapezia are made up from neighbouring viscosity curve differences and their shear rate differences, which are then summed discretely:

$$H_{A+}^{\star} = \frac{1}{2} \sum_{i} \left(\left(\dot{\gamma}_{i+1} - \dot{\gamma}_{i} \right) \left(\eta_{1} \left(\dot{\gamma}_{i} \right) - \eta_{2} \left(\dot{\gamma}_{i} \right) + \eta_{1} \left(\dot{\gamma}_{i+1} \right) - \eta_{2} \left(\dot{\gamma}_{i+1} \right) \right) \right)$$

for
$$\dot{\gamma}_i < \dot{\gamma}_a$$
 (2)

$$\begin{split} & \dot{\mathcal{H}_{A-}} = \frac{1}{2} \Big| \sum_{i} \Big(\big(\dot{\gamma}_{i+i} - \dot{\gamma}_{i} \big) \Big(\eta_{i} \big(\dot{\gamma}_{i} \big) - \eta_{z} \big(\dot{\gamma}_{i} \big) + \eta_{i} \big(\dot{\gamma}_{i+i} \big) - \eta_{z} \big(\dot{\gamma}_{i+1} \big) \Big) \Big) \Big| \\ & \textit{for } \dot{\gamma}_{a+i} < \dot{\gamma}_{i} < \dot{\gamma}_{b} \end{split} \tag{3}$$

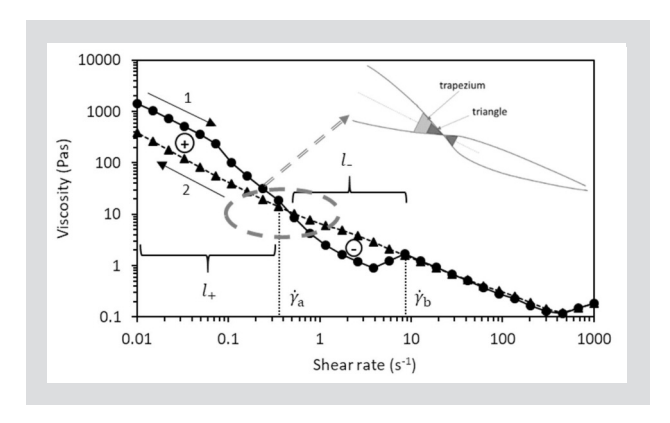


Figure 2: Typical flow curve of an MFC suspension characterised in this work, showing the positive (+) and negative (-) defined hystereses. The insert shows schematically the application of trapezia and triangles to determine the hysteresis

with H_{A+}^* and H_{A-}^* being the positive and negative absolute trapezia sum, respectively, and $\eta_1(\dot{\gamma_1})$ and $\eta_2(\dot{\gamma_1})$ being the viscosity of flow curve 1 and 2 at the shear rate $\dot{\gamma_1}$. To capture also the rates of change of area at the crossing of the viscosity curves, the respective area adjoining either side the boundary with the crossing point, i.e. that spanned by the shear rates before and after the crossing point, can be expressed as two triangles (each equivalent to a trapezium with one side zero length), and thus used to approximate the area growth each side of the crossing point as:

$$H_{A+}^{"} = \frac{\eta_1(\dot{\gamma}_a) - \eta_2(\dot{\gamma}_a)}{2} h \tag{4}$$

$$H_{A-}^{"} = \left| \frac{\eta_{1}(\dot{\gamma}_{a+1}) - \eta_{2}(\dot{\gamma}_{a+1})}{2} \left(\left(\dot{\gamma}_{a+1} - \dot{\gamma}_{a} \right) - h \right) \right| \tag{5}$$

$$h = \frac{(\dot{\gamma}_{a+1} - \dot{\gamma}_a)(\eta_1(\dot{\gamma}_a) - \eta_2(\dot{\gamma}_a))}{(\eta_1(\dot{\gamma}_a) - \eta_2(\dot{\gamma}_a)) + (\eta_2(\dot{\gamma}_{a+1}) - \eta_1(\dot{\gamma}_{a+1}))}$$
(6)

with H_{A+}^{**} and H_{A-}^{**} being the positive and negative absolute triangle and h being the height of the positive triangle. The respective trapezia sum and triangle are summed together to get the positive H_{A+} and negative H_{A-} absolute hysteresis, respectively:

$$H_{A+} = H_{A+}^{*} + H_{A+}^{**} \tag{7}$$

$$H_{A-} = H_{A-}^* + H_{A-}^{**} \tag{8}$$

The second method uses the same approach as used for the absolute hysteresis, but the trapezium areas are normalised by the mean viscosity that is defined by the two viscosity pairs (the two parallel sides of the trapezia):

$$\dot{H_{N+}} = 2\sum_{i} \left(\frac{\left(\dot{\gamma}_{i+i} - \dot{\gamma}_{i} \right) \left(\eta_{1} \left(\dot{\gamma}_{i} \right) - \eta_{2} \left(\dot{\gamma}_{i} \right) + \eta_{1} \left(\dot{\gamma}_{i+1} \right) - \eta_{2} \left(\dot{\gamma}_{i+1} \right) \right)}{\eta_{1} \left(\dot{\gamma}_{i} \right) + \eta_{2} \left(\dot{\gamma}_{i} \right) + \eta_{1} \left(\dot{\gamma}_{i+1} \right) + \eta_{2} \left(\dot{\gamma}_{i+1} \right)} \right) \right)$$

for
$$\dot{\gamma}_i < \dot{\gamma}_a$$
 (9)

$$H_{N-}^{\star} = 2 \left| \sum_{i} \left(\frac{\left(\dot{\gamma}_{i+i} - \dot{\gamma}_{i}\right) \left(\eta_{i}\left(\dot{\gamma}_{i}\right) - \eta_{2}\left(\dot{\gamma}_{i}\right) + \eta_{1}\left(\dot{\gamma}_{i+i}\right) - \eta_{2}\left(\dot{\gamma}_{i+i}\right)\right)}{\eta_{1}\left(\dot{\gamma}_{i}\right) + \eta_{2}\left(\dot{\gamma}_{i}\right) + \eta_{1}\left(\dot{\gamma}_{i+1}\right) + \eta_{2}\left(\dot{\gamma}_{i+1}\right)} \right) \right|$$

for
$$\dot{\gamma}_{a+i} < \dot{\gamma}_i < \dot{\gamma}_b$$
 (10)

with H_{N+} * and H_{N-} * being the positive and negative normalised trapezia sum, respectively. Also, the triangle areas, as before, representing the area growth behavior either side of the crossing point are normalised using the following formulae:

$$H_{N+}^{"} = \frac{2H_{A+}^{"}}{\frac{\eta_{1}(\dot{\gamma}_{a}) + \eta_{2}(\dot{\gamma}_{a})}{2} + \left(\eta_{1}(\dot{\gamma}_{a}) + h\frac{\eta_{1}(\dot{\gamma}_{a+1}) + \eta_{1}(\dot{\gamma}_{a})}{\dot{\gamma}_{a+1} - \dot{\gamma}_{a}}\right)}$$
(11)

$$H_{N-}^{"} = \left| \frac{2H_{A-}^{"}}{\frac{\eta_{1}(\dot{\gamma}_{a+1}) + \eta_{2}(\dot{\gamma}_{a+1})}{2} + \left(\eta_{1}(\dot{\gamma}_{a}) + h\frac{\eta_{1}(\dot{\gamma}_{a+1}) + \eta_{1}(\dot{\gamma}_{a})}{\dot{\gamma}_{a+1} - \dot{\gamma}_{a}}\right)} \right|$$
(12)

with $H_{N_+}^{**}$ and $H_{N_-}^{**}$ being the positive and negative normalised triangle hysteresis area. The trapezia and triangle areas are again summed up to give:

$$H_{N+} = H_{N+}^* + H_{N+}^{**} \tag{13}$$

$$H_{N-} = H_{N-}^{*} + H_{N-}^{*} \tag{14}$$

with H_{N+} and H_{N-} being the positive and negative normalised hysteresis, respectively. The third method aims to describe the data as it is presented in a log-log plot (Figure 2), so instead of looking at viscosity differences, the viscosity ratios are evaluated. As for the previously described methods, the hystereses are calculated by summing up trapezia and triangle areas. The calculation for this approach is simplified because the height of the trapezia is constant. To ease the calculations further, the constant length was set to 1, and the respective term for the height was removed completely from the calculations:

$$H_{R+}^{*} = \frac{1}{2} \sum_{i} \left[log \left(\frac{\eta_{i}(\dot{\gamma}_{i})}{\eta_{2}(\dot{\gamma}_{i})} \right) + log \left(\frac{\eta_{i}(\dot{\gamma}_{i+1})}{\eta_{2}(\dot{\gamma}_{i+1})} \right) \right]$$

$$for \ \dot{\gamma}_{i} < \dot{\gamma}_{a}$$

$$(15)$$

$$H_{R-}^* = \frac{1}{2} \left[\sum_{i} \left[log \left(\frac{\eta_1(\dot{\gamma}_i)}{\eta_2(\dot{\gamma}_i)} \right) + log \left(\frac{\eta_1(\dot{\gamma}_{i+1})}{\eta_2(\dot{\gamma}_{i+1})} \right) \right] \right]$$

for
$$\dot{\gamma}_{a+1} < \dot{\gamma}_i < \dot{\gamma}_b$$
 (16)

with H_{R+}^* and H_{R-}^* being the positive and negative relative trapezia sum, respectively. The positive and negative relative triangle areas $(H_{R_{+}}^{**}, H_{R_{-}}^{**})$, as well as the positive and negative relative hystereses (H_{R+}, H_{R-}) were then calculated as follows:

$$H_{N+}^{"} = \frac{2H_{A+}^{"}}{\frac{\eta_{1}(\dot{\gamma}_{a}) + \eta_{2}(\dot{\gamma}_{a})}{2} + \left[\eta_{1}(\dot{\gamma}_{a}) + h\frac{\eta_{1}(\dot{\gamma}_{a+1}) + \eta_{1}(\dot{\gamma}_{a})}{\dot{\gamma}_{a+1} - \dot{\gamma}_{a}}\right]} H_{R+}^{"} = \frac{log\left(\frac{\eta_{1}(\dot{\gamma}_{a})}{\eta_{2}(\dot{\gamma}_{a})}\right)}{2} \frac{log\left(\frac{\eta_{1}(\dot{\gamma}_{a})}{\eta_{2}(\dot{\gamma}_{a})}\right)}{log\left(\frac{\eta_{1}(\dot{\gamma}_{a})}{\eta_{2}(\dot{\gamma}_{a})}\right) - log\left(\frac{\eta_{1}(\dot{\gamma}_{a+1})}{\eta_{2}(\dot{\gamma}_{a+1})}\right)}$$

$$(17)$$

$$H_{N_{-}}^{"} = \begin{vmatrix} \frac{2H_{A_{-}}^{"}}{\frac{\eta_{1}(\dot{\gamma}_{a+1}) + \eta_{2}(\dot{\gamma}_{a+1})}{2} + \left[\eta_{1}(\dot{\gamma}_{a}) + h\frac{\eta_{1}(\dot{\gamma}_{a+1}) + \eta_{1}(\dot{\gamma}_{a})}{\dot{\gamma}_{a+1} - \dot{\gamma}_{a}} \right]} \end{vmatrix} \\ H_{R_{-}}^{"} = \frac{log\left(\frac{\eta_{1}(\dot{\gamma}_{a+1})}{\eta_{2}(\dot{\gamma}_{a+1})}\right)}{2} \left[1 - \frac{log\left(\frac{\eta_{1}(\dot{\gamma}_{a})}{\eta_{2}(\dot{\gamma}_{a})}\right)}{log\left(\frac{\eta_{1}(\dot{\gamma}_{a})}{\eta_{2}(\dot{\gamma}_{a})}\right) - log\left(\frac{\eta_{1}(\dot{\gamma}_{a+1})}{\eta_{2}(\dot{\gamma}_{a+1})}\right)}{log\left(\frac{\eta_{1}(\dot{\gamma}_{a})}{\eta_{2}(\dot{\gamma}_{a})}\right) - log\left(\frac{\eta_{1}(\dot{\gamma}_{a+1})}{\eta_{2}(\dot{\gamma}_{a+1})}\right)}{log\left(\frac{\eta_{1}(\dot{\gamma}_{a})}{\eta_{2}(\dot{\gamma}_{a})}\right) - log\left(\frac{\eta_{1}(\dot{\gamma}_{a+1})}{\eta_{2}(\dot{\gamma}_{a+1})}\right)}{log\left(\frac{\eta_{1}(\dot{\gamma}_{a})}{\eta_{2}(\dot{\gamma}_{a})}\right) - log\left(\frac{\eta_{1}(\dot{\gamma}_{a})}{\eta_{2}(\dot{\gamma}_{a+1})}\right)}{log\left(\frac{\eta_{1}(\dot{\gamma}_{a})}{\eta_{2}(\dot{\gamma}_{a})}\right) - log\left(\frac{\eta_{1}(\dot{\gamma}_{a})}{\eta_{2}(\dot{\gamma}_{a})}\right) - log\left(\frac{\eta_{1}(\dot{\gamma}_{a})}{$$

$$H_{R+} = H_{R+}^* + H_{R+}^{**} \tag{19}$$

$$H_{R-} = H_{R-}^{*} + H_{R-}^{**} \tag{20}$$

The fourth method is a very simple alternative to calculate the relative hysteresis. Hence, instead of calculating the hysteresis areas, only the viscosity ratios are summed up (that is the same as summing up the log quotient of the viscosities):

$$H_{RS+} = \sum_{i} \left(log \left(\frac{\eta_{i}(\dot{\gamma}_{i})}{\eta_{2}(\dot{\gamma}_{i})} \right) \right) \qquad \text{for } \dot{\gamma}_{i} \leq \dot{\gamma}_{a}$$
(21)

$$H_{RS-} = \left| \sum_{i} \left[log \left(\frac{\eta_{i}(\dot{\gamma}_{i})}{\eta_{2}(\dot{\gamma}_{i})} \right) \right] \qquad for \ \dot{\gamma}_{a+i} < \dot{\gamma}_{i} < \dot{\gamma}_{b}$$
(22)

with H_{RS+} and H_{RS-} being the positive and negative relative hysteresis calculated by the simplified method, respectively. For all the different hysteresis types, a total hysteresis was calculated (sum of the magnitudes of the respective positive and negative hysteresis, H_A , H_R , H_{RS} and H_N , as well as the positive share in % of the total hysteresis $(H_{A+}/H_A, H_{R+}/H_R, H_{RS+}/H_{RS})$ and H_{N+}/H_N . Finally, also the "positioning" of the two different hystereses is characterised: The end of the positive hysteresis $\dot{\gamma}_a$ is defined as the last shear rate where $\eta_1 > \eta_2$ and the end of the negative hysteresis $\dot{\gamma}_{\rm b}$ is defined where $\eta_1 \cong \eta_2$ for the first time after $\eta_1 < \eta_2$. Also, the respective "length" of the hysteresis is described by summing up the log-equidistantly distributed number of point measurements i (for the similarly defined point separation) within a respective hysteresis (I_+, I_-) . Please note that this method leads to a value depending on the acquisition settings of the rheometer. However, as long as the settings are consistently the same within a study, the thus obtained length data can be compared without any problems. The hysteresis parameterising data described above, consisting of nine individual measurements per dilution, are presented in box charts (see e.g. Figure 4a) containing the data median (line), mean (triangle), 25 to 75 percentile (box) and minimum to maximum range (whiskers). The hysteresis position properties data are presented differently because box charts are not suitable. Here, the individual values are shown (hollow diamonds) instead of the percentile box. The mean and median data are presented the same way as described for the other hysteresis data.

Firstly, a normality test (Shapiro-Wilk, 0.05 signifi cance level, Origin 2017) was carried out on the data points within each dilution and given property in order to identify potential grouping effects. Secondly, an analysis of variance test (ANOVA, 0.05 significance level, Origin 2017) was carried out among the different levels of dilution within each property separately. The test not only reveals whether different dilutions (mean values) at a given property are significantly different from each other, but also provides the strength of effect and the test power. For data where a significant difference was identified, a mean comparison test (Tukey, 0.05 significance level, Origin 2017) was carried out additionally to identify which combination of datasets were different. As the hysteresis position properties (end and length of positive and negative hysteresis) appear to be not normally distributed and have discrete values, a Kruskal-Wallis test was carried out for these data instead [32].

3 RESULTS AND DISCUSSION

3.1 MORPHOLOGICAL MODEL

The presence of the so called "rheological hysteresis" in complex fluids is well known and attributed to the time-dependence of their viscosity, i.e. their thixotropy [33]. The reason for thixotropic behavior is very often a morphological change of the fluid that is induced by deformation (shear), e.g. orientation of macromolecules, phase separation or other structural reorganisations. MFC suspensions are well known also to undergo morphological changes under flow, leading for instance to the typical discontinuous shear thinning behavior [13, 31, 34], but also to hysteresis [9, 17, 19, 35]. The hysteresis between the increasing shear rate viscosity curve and the decreasing shear rate viscosity curve is typically explained by different structures that depend on the shear history and the characteristically long relaxation times (= the time needed for a non-equilibrium structure induced at a given shear rate to transform back to its equilibrium structure). For the following discussions, it should be noted that the mechanistic model of Martoïa et al. [9] is followed, and that this is well supported by, for example, Karppinen et al. [31] and Schenker et al. [13] for the shear rate increase part of the flow curve. In short, they explain the observed positive hysteresis (present at lower shear rates, as seen in this work, Figure 2) as originating because the initial structure (low shear rates of the increasing shear rate curve) is homogeneous, and has, therefore, a higher viscosity compared to the more flocculated structure that was induced by intermediate shear rates (on the decreasing shear rate ramp). It is apparent that the negative hysteresis is mainly caused by the "dip" of the increasing shear rate flow curve (Figure 2). Following the argumentation of Schenker et al. [13], based on findings of Karppinen et al. [31], this behavior is related to the formation of loosely bound flocs and water-rich voids, reducing overall viscosity. It is interesting to note, that there is no such dip (or a lot less pronounced one) at the same shear rates in the decreasing shear rate ramp. So, it is possible to assume that the flocculated structure that is induced by the high shear rates differs from the (flocculated) structure at the lower shear rates.

3.2 FLOW CURVES

Figure 3 shows the averaged flow curves of the 1, 1.5, and 2 wt% MFC suspensions investigated in this work. Positive as well as negative hysteresis areas can be seen in all curves, and it is apparent that the negative hysteresis becomes smaller with increasing solids content. As is to be expected, the overall viscosity levels increase

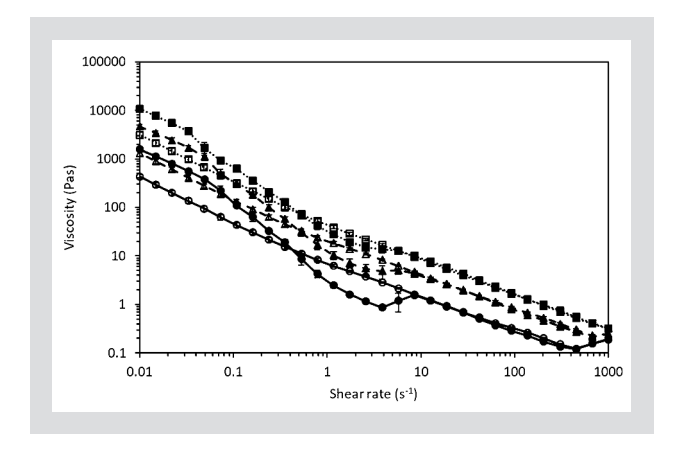


Figure 3: Flow curves of averaged data for 1 (circles), 1.5 (triangles), and 2 wt% (squares) MFC suspensions including standard deviations (error bars). The full symbols represent the data during shear rate increase and the hollow symbols represent the data during shear rate decrease, respectively.

with the solids content. The quantitative evaluation of the hysteresis of these flow curves, as well as the potential underlying morphological reason will be discussed in the next section.

3.3 INFLUENCE OF SOLIDS CONTENT ON HYSTERESIS PROPERTIES

When comparing the data spread in the following Figures (Figure 4 to Figure 6) with the standard deviations shown in Figure 3, they may at first sight appear inconsistent. However, it should be kept in mind that the standard deviation is inversely scaled with the square root of the number of sample points, *n*, so becoming smaller with an increasing number of data points. Thus, the data in the following graphs do not show a standard deviation, but quantiles, and maximum and minimum values (so the complete data spread). It is very apparent from the data in Figure 4a that the positive absolute hysteresis H_{A+} increases significantly (Table 1) with the solids content, keeping in mind the logarithmic scale. This is not surprising if one considers the overall viscosity increase with the solids content (Figure 3) and that H_{A+} is calculated from absolute viscosity values without any normalisation (Equations 2 to 8). Keeping this in mind, at first the trend observed for the negative absolute hysteresis H_{A-} appears counterintuitive (Figure 3 and Figure 4b). This can, however, be explained straightforwardly, once again, in terms of the strongly changing overall viscosities. Also for the same reason, the total absolute hysteresis H_A , Figure 4c, as well as the positive share H_{A+}/H_A , Figure 4d, are basically just depending on the positive absolute hysteresis. To undertake a separate evaluation of these properties is, therefore, questionable.

As seen in the discussion before, the absolute hysteresis data are very strongly dominated by the initial, low shear rate data due to the strongly shear thinning and solid content-depending nature of MFC suspensions. To be able to decouple this effect, the normalisation was introduced according to Equations 9 to 14. These data are presented in Figure 5. The dependency

of the positive normalised hysteresis H_{N+} on the solids content seems to have vanished (there was no significant difference found by the ANOVA test, Table 1). This contrasts with the H_{A+} data, yet it reflects directly the situation seen in the log-log flow curve diagram (Figure 3). Furthermore, the normalised data show clear trends (statistically significant, Table 1) that an increase in solids content leads to a decrease in the negative and total normalised hystereses H_{N-} and H_{N} (Figure 5b and c) and an increased share of the positive normalised hysteresis H_{N+}/H_{N} (Figure 5d). The normalisation proves to be very useful with respect to making the hysteresis data of different dilutions directly comparable.

It is apparent, that the normalised hysteresis data (Figure 5) and the relative hysteresis data (Figure 6) have very alike trends. This is supported by the statistical test data (Table 1), except for the positive hysteresis where the normalised data show no trend with the suspension solids content, but the relative data do. However, the low power of the ANOVA test for H_{N+} already indicates that the chance is high, that a significant difference is not found by the test. Furthermore, the strength of effect for the positive relative and normalised hysteresis is small (in general, but also compared to the rest of the tested data). This indicates that even if there is a trend, the dependency of H_{N+} and H_{R+} on the suspension solids content will be small. As is to be expected, the relative hysteresis data, like the normalised hysteresis data, are not affected by the overall viscosity levels, because of their relative character. It was found that the relative hysteresis data obtained by the simplified method (line summation) correlate very well (r² > 0.99 for all data sets) with the relative hysteresis data obtained by the extensive procedure (Figure 7), so no box charts are provided. The ANOVA test results are almost identical for both approaches (Table 1) as well, legitimising the simplified procedure.

As mentioned in the methods section, the data of the hysteresis positioning were not normally distributed (non-Gaussian), and, therefore, not presented as

Property	ANOVA result $(\alpha = 0.05)$	Test power	Effect strength	Significant pair-wise comparisor ($\alpha = 0.05$)
H _{A+}	Significantly different	1	0.92	All
H _A .	Significantly different	0.89	0.37	1 - 1.5 wt%, 1 - 2 wt%
H _A	Significantly different	1	0.92	All
H _{A+} /H _A	Significantly different	1	0.63	All
H _{N+}	Not significantly different	0.35	0.13	
H _N -	Significantly different	1	0.70	All
H _N	Significantly different	1	0.71	All
H _{N+} /H _N	Significantly different	0.98	0.48	1-2
H _{R+}	Significantly different	0.9	0.32	1 - 2 wt%, 1.5 - 2 wt%
H _R .	Significantly different	1	0.74	All
H_R	Significantly different	1	0.72	All
H _{R+} /H _R	Significantly different	1	0.66	1 - 1.5 wt%, 1 - 2 wt%
H _{RS+}	Significantly different	0.78	0.30	1 – 2 wt%
H _{RS} .	Significantly different	1	0.74	All
H _{RS}	Significantly different	1	0.70	All
H _{RS+} /H _{RS}	Significantly different	1	0.66	1 - 1.5 wt%, 1 - 2 wt%

Table 1: Statistical test decisions including the ANOVA test power and strength of effect for hysteresis data.

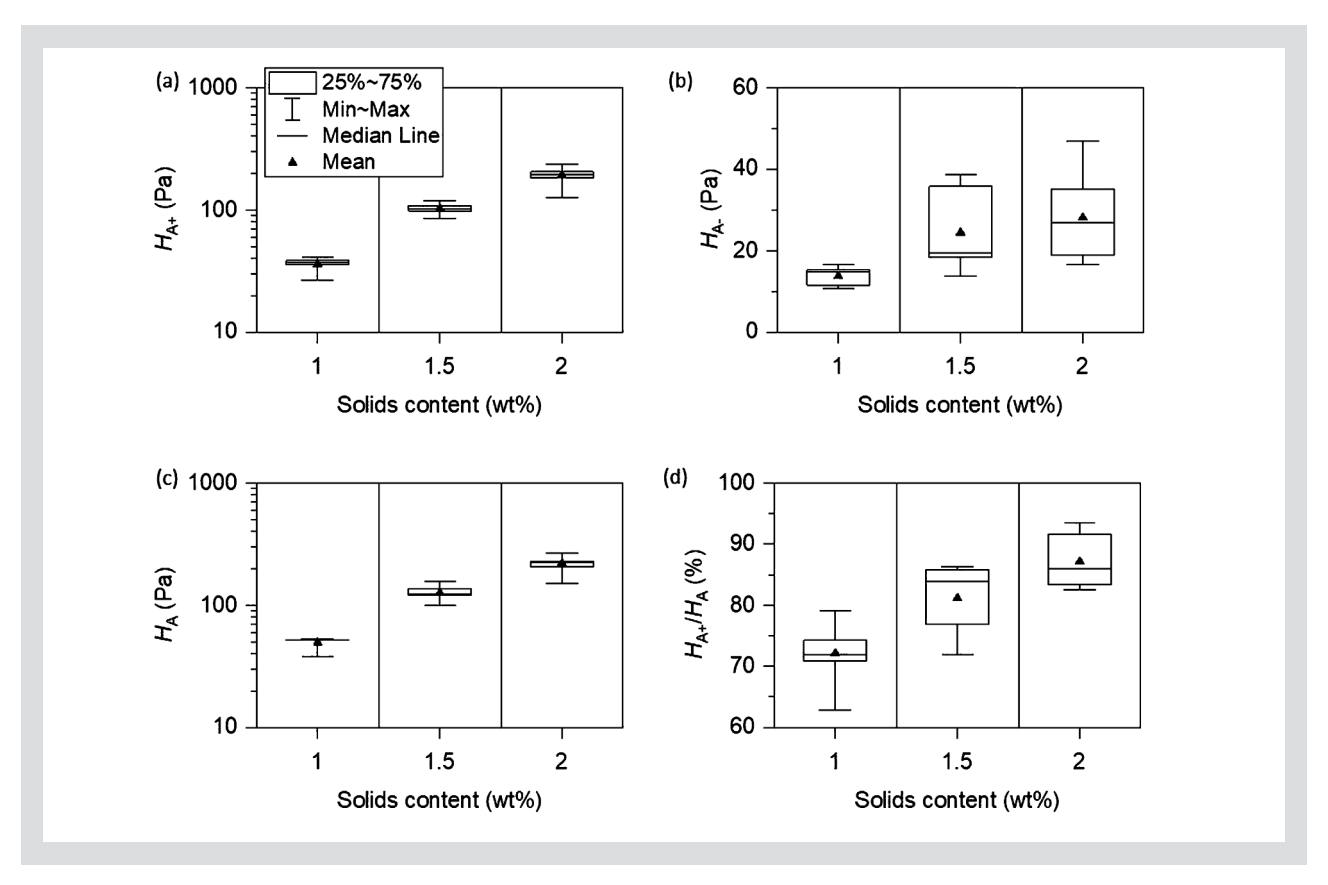


Figure 4: Box charts of absolute hysteresis data: (a) positive absolute hysteresis (HA+), (b) negative absolute hysteresis (HA-), (c) total absolute hysteresis (HA) and (d) positive absolute hysteresis in respect to the total absolute hysteresis (HA+/HA). Please note that the scales for HA+ and HA are logarithmic.

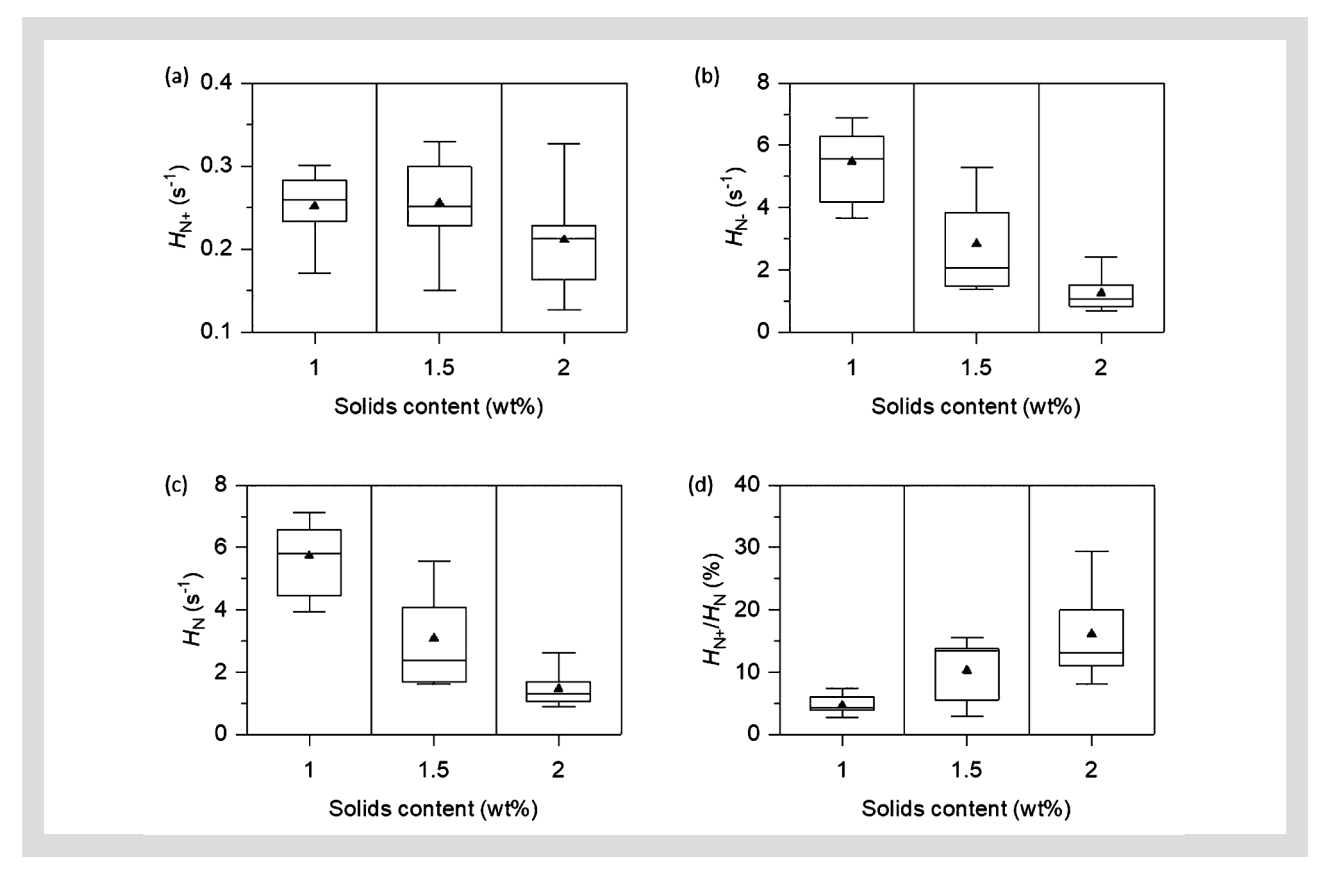


Figure 5: Box charts of normalised hysteresis data: (a) positive normalised hysteresis (HN+), (b) negative normalised hysteresis (HN), and (d) fraction of positive normalised hysteresis in respect to the total normalised hysteresis (HN+/HN).

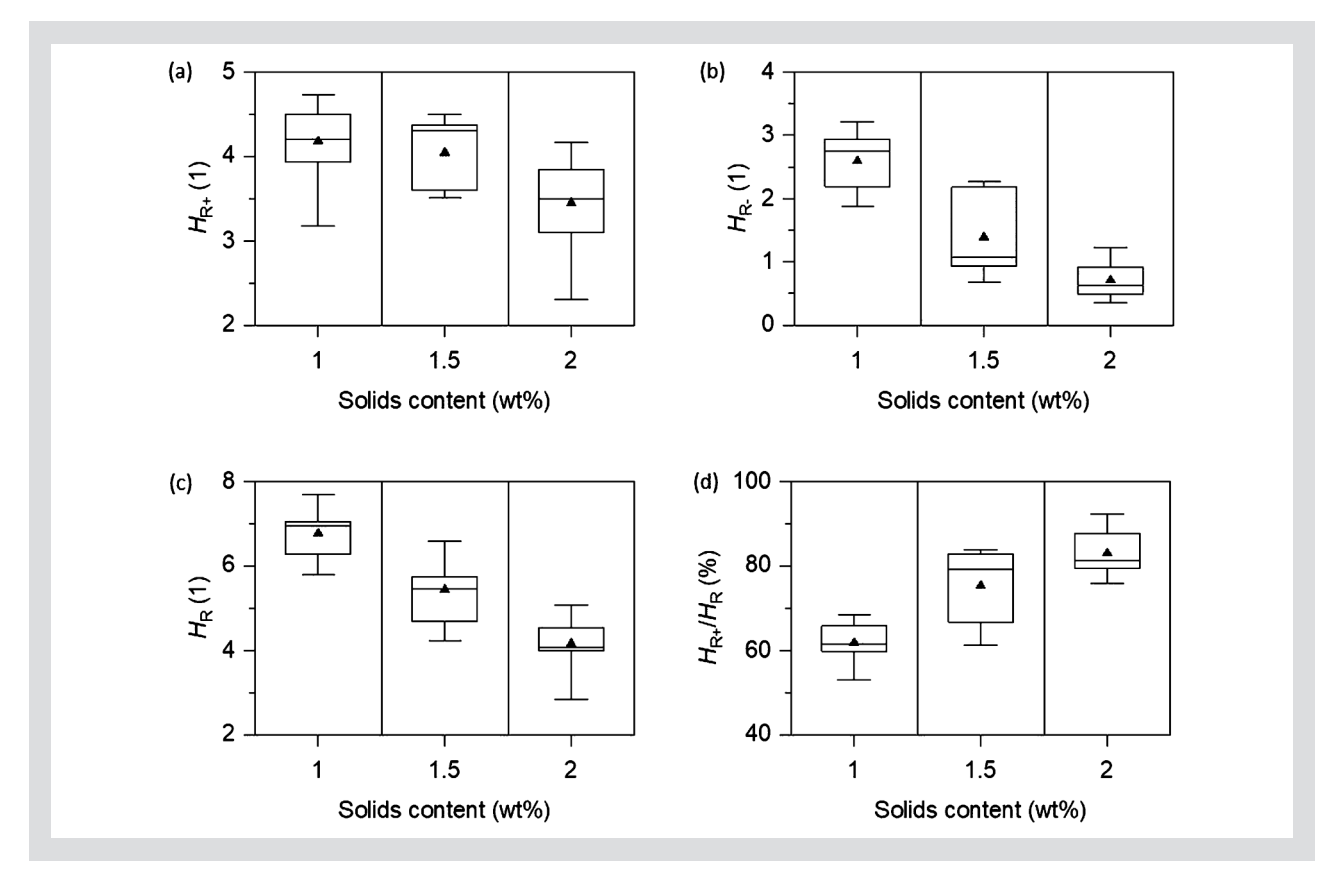


Figure 6: Box charts of relative hysteresis data: (a) positive relative hysteresis (HR+), (b) negative relative hysteresis (HR-), (c) total relative hysteresis (HR), and (d) fraction of positive relative hysteresis in respect to the total relative hysteresis (HR+/HR).

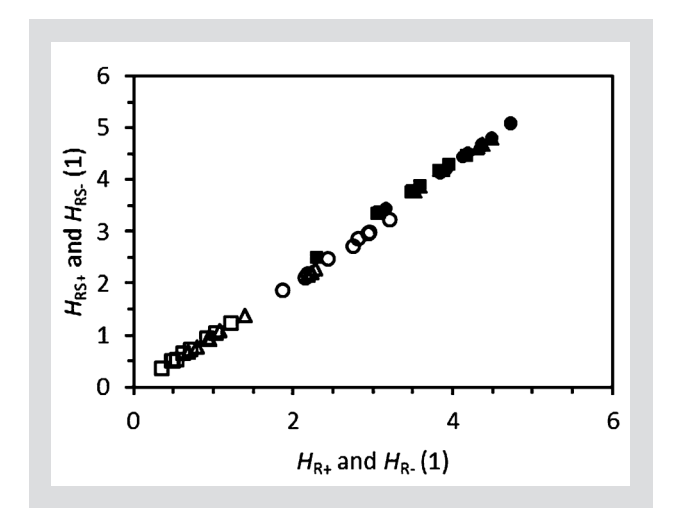


Figure 7: Comparison of positive (full symbols) and negative (hollow symbols) relative hysteresis data obtained by the regular method (HR+ and HR-) and the simplified method (HRS+ and HRS-). Circles represent the 1 wt% suspension data, triangles the 1.5 wt% data and the squares the 2 wt% data.

box charts (Figure 8). As all these data are based on shear rate values that are predefined by the rheometer software and the measurement settings, they are discrete. The different data groups that are apparent next to each other in Figure 8a and b, for instance, represent data of adjacent pre-set measurement shear rates (0.24, 0.36, and 0.53 s⁻¹ for $\dot{\gamma}_a$, respectively, 3.86, 5.74, and 8.53 s⁻¹ for $\dot{\gamma}_b$). For all properties except the end of the positive hysteresis, and corresponding hysteresis

length $(\dot{\gamma}_a, l_+)$, both of which must have the same test results anyway in a parametrised test, a significant difference was found for the different solids contents (Table 2). The pair-wise test only identified a difference between 1 and 2 wt% for all these properties. Looking at the data directly then shows, that the median values of those data-pairs are just one value apart from each other, so the effect strength is low. Due to the nature of the present data, as discussed above, it is difficult to identify a potential trend. Yet, with some caution, it may be hypothesised that the end and the length of the negative hysteresis $(\dot{\gamma}_b, l_-)$ as well as the total hysteresis length l decrease with increasing solids content, provided the increase in solids content is large enough.

Property	Kruskal-Wallis result	Significant pair-wise comparisons	
	$(\alpha = 0.05)$	$(\alpha = 0.05)$	
γ̈́a	Not significantly different		
1+	Not significantly different		
$\dot{\gamma}_{\mathrm{b}}$	Significantly different	1 – 2 wt%	
1.	Significantly different	1 – 2 wt%	
1	Significantly different	1 – 2 wt%	
1+/1	Significantly different	none	

Table 2: Statistical test decisions for the hysteresis positioning data. Even though the test for the fractional contribution of the positive length in respect to total hysteresis length (I_+ /I) has provided a decision in favor that there is a significant difference among the data sets for the different solids contents, the pair-wise test, however, did not identify a significantly different dataset.

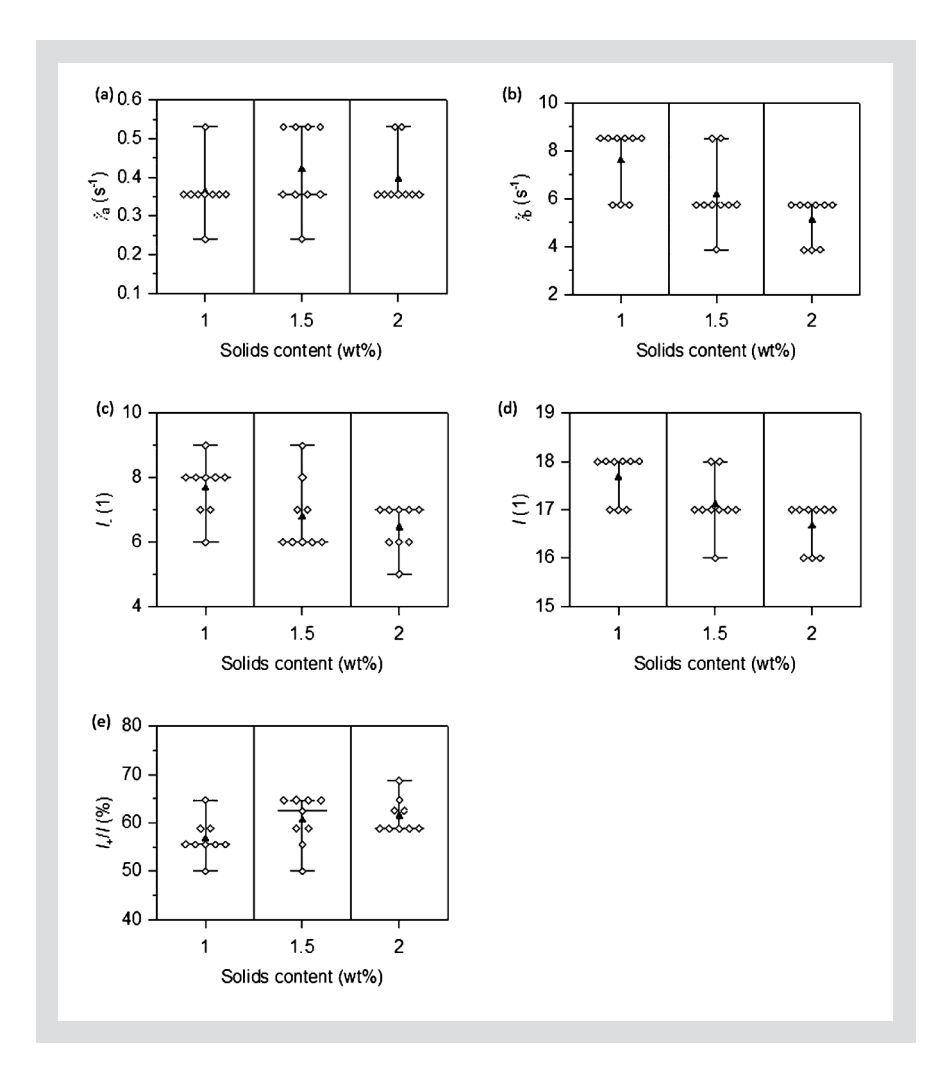


Figure 8: Hysteresis positioning data: (a) end of positive hysteresis ($\dot{\gamma}_a$), (b) end of negative hysteresis ($\dot{\gamma}_b$), (c) length of negative hysteresis (!.) and total hysteresis length (!), and (e) fraction of positive hysteresis in relation to the total hysteresis length (l_+ /l). The positive length data (l_+) are not presented because the distribution is identical to $\dot{\gamma}_a$.

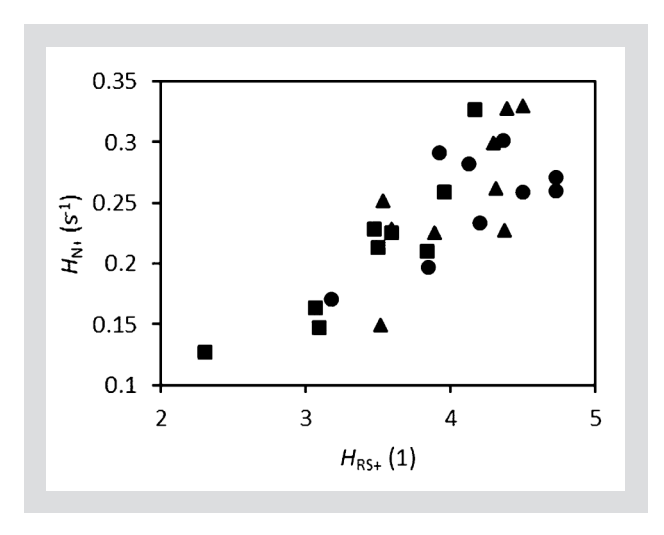


Figure 9: Comparison of positive normalized hysteresis and positive relative hysteresis data (obtained by the simplified calculation) of 1 wt% (circles), 1.5 wt% (triangles) and 2 wt% suspensions (squares).

3.4 LEARNINGS

Due to its strong dependency on the suspension solids content, the absolute hysteresis properties may be impractical for hysteresis discussions. Due to the strongly shear thinning nature of MFC suspensions, the hysteresis data at low shear rates are dominating the overall properties. On the one hand, comparisons between positive and negative hysteresis become bypassed, and on the other hand even within the positive hysteresis, the overall properties are mostly dominant within the very low shear rate region. Due to the high sensitivity, the absolute hysteresis may probably be used to differentiate between different solids contents. However, there are other more direct and equally sensitive rheological properties providing the same information [13]. The normalisation of the hysteresis data was successful in describing the data accurately from the point of view of their expression

on the log-log flow-curve graphs. This is not only supported by visual observation, but also indirectly evidenced by the very good correlation between the relative hysteresis data and the actual quantified log-log plot data. The simplified calculation of the relative hysteresis has shown to be accurate enough, so presents a legitimate way of obtaining the relative hysteresis data with less effort.

If one compares the normalised hysteresis with the relative hysteresis data, exemplified here with the positive hysteresis (Figure 9), it is apparent that the correlation is not very good. The reason for this can be expected from the hysteresis calculation procedures: For both the absolute and normalised hysteresis, trapezia and triangles are used as approximations to the real area between the curves. However, as the flow curves mostly follow power laws, there will be inherent errors arising from this approximation. As the log data are used for the relative hysteresis calculation, the power law behavior is transformed to linear functions, and so trapezia and triangles become better approximations for the data. Therefore, it can be expected, that the relative hysteresis data are more accurate than the ab-

solute and normalised data, and should be used in preference. Having a small data variation in respect to the hysteresis positioning may indicate that the number of contributing point measurements within the flow curves are too few. With the settings used in this work, each successive measured shear rate is about 150% of the previous one. So, the span may be indeed too large to get a sufficiently closely stepped distribution. If enough points would be added, the length data should then follow a normal distribution, as it is based on logarithmic shear rate data. As the number of point measurements is determined by the flow curve parameters, it may easily be increased by just changing those parameters adequately. If the span of shear rates should remain the same, this, of course, also means a significantly increased experimental data collection time.

3.5. HYSTERESIS PROPERTIES DEPENDENCE ON SOLIDS CONTENT

As the positive relative hysteresis apparently does not change strongly with solids content, it may be hypothesised that the morphology at the end of the decreasing shear rate ramp-down is homomorphic with its structure at the beginning of the increasing shear rate ramp at low shear rates. The self-similarity in this case is interpreted in such a way that the amount and types of interactions between the fibrils in the primary shear state and within the structure at the end of the second flow curve scale with each other, independent of the solids content. This would also imply, that there is only a minor release of free water in the structure at the end of the second flow curve, because otherwise it could be expected that the positive hysteresis is increased more pronouncedly with a decrease of the solids content (higher potential availability of water). Since precisely this free water behavior is seen for the negative relative hysteresis, it is likely that there is a significant water release in the transition zone during the increasing shear rate ramp-up, probably originating from a very pronounced flocculation as seen by Karppinen et al. [31]. As a lower solids content means more water to be freed, the negative relative hysteresis increases with decreasing suspension solids content. Following the proposed mechanistic model by Martoïa et al. [9], the positive hysteresis is attributed to the difference between the initial structure and the finally flocculated structure that is induced and recovering at the end of the decreasing shear rate ramp-down. However, since the applicability of the morphological models proposed by Martoïa et al. and Karppinen et al. to the experimental setup discussed here cannot be taken for granted ad hoc, the above discussion remains speculative and requires further proof, e.g. by rheo-optical measurements.

3.6. COMPARISON WITH OTHER MFC SUSPENSION HYSTERESIS DATA

Comparing a typical hysteresis obtained in this work, characterised by a positive and negative contribution $\eta_1(\dot{\gamma}_i) > \eta_2(\dot{\gamma}_i)$ and $\eta_1(\dot{\gamma}_i) < \eta_2(\dot{\gamma}_i)$, respectively, with examples reported by others [9, 17, 19, 35], reveals some significant differences. Very apparently, all of them only report one type of hysteresis, either positive or negative according to our here-used definition. Whereas it is not clear if it is positive or negative in the works by Jia et al. and Agoda-Tandjawa et al. [17, 35], it is reported to be positive by Martoïa et al. [9] and to be negative in the work by lotti et al. [19]. A direct comparison may be somewhat critical, as the MFC suspensions were manufactured differently (here: grinding; lotti et al.: homogenised; and Martoïa et al.: enzymatic pre-treatment and grinding) and, therefore, may inherently have a different flow curve profile. Nonetheless, all those different hystereses seem to be strikingly similar when the dilutions and measurement conditions are considered in addition, and a qualitative comparison should be possible. The following apparent differences should be especially highlighted:

- The MFC suspensions were pre-sheared in the cited experiments and was not pre-sheared in the current work (Martoïa et al. [9]: 1 000 s⁻¹ for 60 s, no mentioning of rest time, lotti et al. [19]: 50 s⁻¹ for 120 s and 600 s rest time)
- The measurement systems were different (Couette in Martoïa et al. [9], parallel plate in lotti et al. [19] and vane in serrated cup in our work)
- The solids contents (1 to 4 wt% in lotti et al. [19], even though only the 1 wt% flow curve was discussed in detail, and only 2 wt% in Martoïa et al. [9])
- The acquisition times were fixed in the cited works (lotti et al. [19]: 10 s, Martoïa et al. [9]: 50 s) and was automated in this work (min. of 15.2 s)
- The shear rate ranges were different (0.1 to 1000 s⁻¹ and vice versa in lotti et al.'s setup, 0.001 to 1000 s⁻¹ and vice versa in Martoïa et al. [9] and we used 0.01 to 1000 s⁻¹ and vice versa).

Based on those differences, the absence of the positive hysteresis in lotti et al.'s [19] data may be explained by the pre-shearing. This may already have introduced a flocculated structure, which did not relax to recover the homogeneous structure during the rest phase, and therefore, the low shear viscosity during the shear rate ramp-up was already low (equal to the low shear viscosity of the shear rate ramp-down), and so no positive hysteresis is seen. The absence of the negative hysteresis in Martoïa et al.'s work may have several reasons. Firstly, as shown in the work of Schenker et al. [13], the vane spindle (VS) system appears to lead to a stronger

flocculation at intermediate shear rates, leading to a deeper viscosity drop during the shear rate ramp-up compared to smooth cylinder roughened cup systems as used by Martoïa et al. [9]. When comparing the flow curves obtained by different measuring systems through Schenker et al.'s work [13], the smooth system should be considered for Martoïa et al.'s data [9]. This is based on observations (unpublished), that the condition of the moving geometry (typically the inner part in modern shear rheometers using Couette type cells) is the main contributor to the overall flow curve. Secondly, as shown in this work, the negative hysteresis seems to become smaller with increasing solids contents, and as Martoiä et al. [9] only provided data at 2 wt% that can be considered as "high" solids content only, and so only a small hysteresis would be expected anyway. The above comparison shows the critical influence of the rheometer set-up and measurement parameters. Yet, still, qualitative comparisons, like the one above, can be made when these conditions are fully considered. To do so, it is of critical importance to know all the relevant measurement parameters, as they strongly affect the obtained data. We, therefore, would highly encourage peers to provide such parameters when publishing rheological data in the context of similar systems, especially those including micro and nanofibrillated cellulose suspensions.

4 CONCLUSIONS

In this paper, we have set out to provide a procedure to quantify the hysteresis data of flow curves that are typically observed in MFC suspensions. At low shear rates (0.01 up to about 1 s⁻¹), a "positive hysteresis" area was found where the viscosity of the initial, shear rate increasing flow curve is higher than the viscosity of the following, shear rate decreasing curve. At further increasing shear rates up to about 10 s⁻¹, a "negative hysteresis" area was found, having a reversed order of the viscosities compared to the positive hysteresis. It was shown that a viscosity depending normalisation of the data is necessary to be able to compare directly data of MFC suspensions of different solids content. Whereas the positive normalised hysteresis decreased only slightly with an increasing suspension solids content, the negative normalised hysteresis decreased very strongly, as supported by statistical test results. These data show, that MFC suspensions exhibit different morphologies, not only depending on the shear rate, but also on the direction of the shear rate ramp, and, under some conditions, also on the suspension solids content. Finally, hypothetical mechanistic models of the MFC suspensions as a function of shear rate were suggested, based on prior models proposed by other researchers, but remain to be proven. The need to define both measurement geometry and data collection parameters in detail, including collecting sufficient measurement points, is emphasised by the uncertainty identified by statistically relevance testing. However, the same statistical rigor clearly provides confidence the principles applied. Further work is carried out to investigate the influence of the degree of fibrillation of an MFC suspension on this and other rheological properties, to further demonstrate the usefulness of this novel characterisation method.

ACKNOWLEDGEMENTS

Elias Niklaus and Dr. Johannes Kritzinger are acknowledged for their valuable inputs on statistics and supporting discussions. Omya International AG and Fiber-Lean Technologies Ltd. are thanked for their funding.

REFERENCES

- [1] Hubbe MA, Ferrer A, Tyagi P, Yin Y, Salas C, Pal L, Rojas OJ: Nanocellulose in thin film, coatings, and plies for packaging applications: A review, BioResources 12 (2017) 2143 2233.
- [2] Oksman K, Y. A, Mathew AP, Siqueira G, Zhou Q, Butylina S, Tanpichai S, Zhou X, Hooshmand S: Review of the recent developments in cellulose nanocomposite processing, Composites Part A: Appl. Sci. Manufact. 83 (2016) 2–18.
- [3] Boufi S, González I, Delgado-Aguilar M, Tarrès Q, Pèlach MA, Mutjé P: Nanofibrillated cellulose as an additive in papermaking process: A review, Carbohydrate Polymer. 154 (2016) 151–166.
- [4] Nechyporchuk O, Belgacem MN, Bras J: Production of cellulose nanofibrils: A review of recent advances, Ind. Crops Prod. 93 (2016) 2–25.
- [5] Kangas H, Lahtinen P, Sneck A, Saariaho AM, Laitinen O, Hellén E: Characterization of fibrillated celluloses. A short review and evaluation of characteristics with a combination of methods, Nordic Pulp Paper Res. J. 29 (2014) 129-143.
- [6] Spence KL, Venditti RA, Rojas OJ, Habibi Y, Pawlak JJ: A comparative study of energy consumption and physical properties of microfibrillated cellulose produced by different processing methods, Cellulose 18 (2011) 1097–1111.
- [7] Svending P, Skuse D, Phipps J: Micro fibrillated cellulose a new dimension in paper making, Conference on Specialty Papers EU, Manchester UK (2016).
- [8] Desmaisons J, Boutonnet E, Rueff M, Dufresne A, Bras J: A new quality index for benchmarking of different cellulose nanofibrils, Carbohydrate Polymer. 174(2017) 318–329.
- [9] Martoïa F, Perge C, Dumont PJJ, Orgéas L, Fardin MA, Manneville S, Belgacem MN: Heterogeneous flow kinematics of cellulose nanofibril suspensions under shear, Soft Matter 11 (2015) 4742 – 4755.

- [10] Lauri J, Koponen A, Haavisto S, Czajkowski J, Fabritius T: Analysis of rheology and wall depletion of microfibrillated cellulose suspension using optical coherence tomography, Cellulose 24 (2017) 4715 – 4728.
- [11] Haavisto S, Cardona MJ, Salmela J, Powell RL, McCarthy MJ, Kataja M, Koponen Al: Experimental investigation of the flow dynamics and rheology of complex fluids in pipe flow by hybrid multi-scale velocimetry, Exp. Fluids 58 (2017) 158.
- [12] De Kort DW, Veen SJ, Van As H, Bonn D, Velikov KP, Van Duynhoven PM: Yielding and flow of cellulose microfibril dispersions in the presence of a charged polymer, Soft Matter 12 (2016) 4739 4744.
- [13] Schenker M, Schoelkopf J, Mangin P, Gane PAC: Influence of shear rheometer measurement system selection on rheological properties of microfibrillated cellulose (MFC) suspensions, Cellulose 25 (2017) 961–976.
- [14] Nechyporchuk O, Belgacem MN, Pignon F: Rheological properties of micro-/nanofibrillated cellulose suspensions: Wall-slip and shear banding phenomena, Carbohydrate Polymer. 112 (2014) 432–439.
- [15] Saarinen T, Lille M, Seppälä J: Technical aspects on rheological characterization of microfibrillar cellulose water suspensions, Ann. Trans. Nordic Rheol. Soc. 17 (2009) 121–128.
- [16] Pääkkö M, Ankerfors M, Kosonen H, Nykänen A, Ahola S, Österberg M, Ruokolainen J, Laine J, Larsson PT, Ikkala O, Lindström T: Enzymatic hydrolysis combined with mechanical shearing and high-pressure homogenization for nanoscale cellulose fibrils and strong gels, Biomacromolecules 8 (2007) 1934–1941.
- [17] Agoda-Tandjawa G, Durand S, Berot S, Blassel C, Gaillard C, Garnier C, J.L. D: Rheological characterization of microfibrillated cellulose suspensions after freezing, Carbohydrate Polymer. 8o (2010) 677 – 686.
- [18] Dimic-Misic K, Nieminen K, Gane P, Maloney T, Sixta H, Paltakari J: Deriving a process viscosity for complex particulate nanofibrillar cellulose gel-containing suspensions, Appl. Rheol. 24 (2014) 35616.
- [19] Iotti M, Gregersen OW, Moe S, Lenes M: Rheological studies of microfibrillar cellulose water dispersions, J.Polym. Environ. 19 (2011) 137-145.
- [20] Moberg T, Sahlin K, Yao K, Geng S, Westman G, Zhou Q, Oksman K, Rigdahl M: Rheological properties of nanocellulose suspensions: Effects of fibril/particle dimensions and surface characteristics, Cellulose 24 (2017) 2499 2510.
- [21] Debon SJJ, Wallecan J, Mazoyer J: A rapid rheological method for the assessment of the high pressure homogenization of citrus pulp fibres, Appl. Rheol. 22 (2012) 63919.

- [22] Haavisto S, Salmela J, Jäsberg A, Saarinen T, Karppinen A, Koponen A: Rheological characterization of microfibrillated cellulose suspension using optical coherence tomography, Tappi J. 14 (2015) 291–302.
- [23] Nazari N, Kumar V, Bousfield DW, Toivakka M: Rheology of cellulose nanofibers suspensions: Boundary driven flow, J. Rheol. 60 (2016) 1151–1159.
- [24] Kumar V, Nazari B, Bousfield D, Toivakka M: Rheology of microfibrillated cellulose suspensions in pressure-driven flow, Appl. Rheol. 26 (2016) 43534.
- [25] Kataja M, Haavisto S, Salmela J, Lehto R, Koponen A: Characterization of micro-fibrillated cellulose fiber suspension flow using multi scale velocity profile measurements, Nordic Pulp Paper Res. J. 32 (2017) 473–482.
- [26] Nechyporchuk O, Belgacem MN, Pignon F: Current progress in rheology of cellulose nanofibril suspensions, Biomacromolecules 17 (2016) 2311–2320.
- [27] Saarinen T, Haavisto S, Sorvari A, Salmela J, Seppälä J: The effect of wall depletion on the rheology of microfibrillated cellulose water suspensions by optical coherence tomography, Cellulose 21 (2014) 1261–1275.
- [28] Li M-C, Wu Q, Song K, Lee S, Qing Y, Wu Y: Cellulose nanoparticles: Structure-morphology-rheology relationships, ACS Sust. Chem. Eng. 3 (2015) 821–832.
- [29] Schenker M, Schoelkopf J, Mangin P, Gane P: Rheological investigation of complex micro and nanofibrillated cellulose (MNFC) suspensions: Discussion of flow curves and gel stability, Tappi J. 15 (2016) 405–416.
- [30] Schenker M, Schoelkopf J, Mangin P, Gane P: Rheological investigation of pigmented micro-nano-fibrillated cellulose (MNFC) suspensions: Discussion of flow curves, Tappi International Conference on Nanotechnology for Renewable Materials, Grenoble (2016).
- [31] Karppinen A, Saarinen T, Salmela J, Laukkanen A, Nuopponen M, Seppälä J: Flocculation of microfibrillated cellulose in shear flow, Cellulose 19 (2012) 1807–1819.
- [32] Chan Y, Walmsley RP: Learning and understanding the kruskal-wallis one-way analysis-of-variance-by-ranks test for differences among three or more independent groups, Phys Therap. 77 (1997) 1755 1761.
- [33] Mewis J, Wagner NJ: Thixotropy, Adv. Colloid Interface Sci. 147 (2009) 214–227.
- [34] Saarikoski E, Saarinen T, Salmela J, Seppälä J: Flocculated flow of microfibrillated cellulose water suspensions: An imaging approach for characterisation of rheological behaviour, Cellulose 19 (2012) 647 659.
- [35] Jia X, Chen Y, Shi C, Ye Y, Abid M, Jabbar S, Wang P, Zeng X, Wu T: Rheological properties of an amorphous cellulose suspension, Food Hydrocolloid. 39 (2014) 27–33.

